

Transport in disordered media with spatially nonuniform fields

Harvey Scher, Karen Willbrand, and Brian Berkowitz

Department of Environmental Sciences and Energy Research, Weizmann Institute of Science, Rehovot, Israel

(Received 9 September 2009; revised manuscript received 1 December 2009; published 2 March 2010)

The theoretical treatment of transport in a disordered system in the presence of a system-wide force field $\mathcal{F}(\mathbf{x})$ or spatially varying macroscopic velocity field $\mathbf{v}(\mathbf{x})$ is developed in the framework of continuous time random walk (CTRW). The physical basis of CTRW and related fractional derivative equations relies on a mapping of the aggregate of transition rates $w(\mathbf{s}, \mathbf{s}')$, between sites \mathbf{s} and \mathbf{s}' , in the Master equation describing the system kinetics, onto a joint probability distribution function $\psi(\mathbf{s}, t)$. This distribution is calculated from the ensemble average of a position-dependent functional of $w(\mathbf{s}, \mathbf{s}')$; the procedure is effective when the scale of heterogeneities is much smaller than the system size. However, statistical homogeneity does not hold in the presence of large heterogeneities, which control the macroscopic $\mathbf{v}(\mathbf{x})$, or in the case of an interaction of $\mathcal{F}(\mathbf{x})$ with the transition rates. The transport equation, incorporating large-scale heterogeneity, involves the use of a local ensemble average to obtain a position-dependent $\psi(\mathbf{s}, t; \mathbf{x})$; this determines a memory function, $M(t; \mathbf{x})$, which is convoluted with the advection-dispersion operator. A prototype transport equation for a system with statistical inhomogeneity is developed as an integrodifferential equation. It is solved numerically for particles migrating with a steady-state Darcy velocity $\mathbf{v}(\mathbf{x})$, determined for different permeability fields and boundary conditions. The nature of the solutions as a function of key transport parameters (e.g., a characteristic time t_c) is explored, and solutions are also compared to those of the advection-dispersion equation for $\mathbf{v}(\mathbf{x})$ and to a laboratory experiment. This transport equation is in contrast to the fractional Fokker-Planck equation, which is based on a decoupling of $\mathcal{F}(\mathbf{x})$ or $\mathbf{v}(\mathbf{x})$ with the transition rates $w(\mathbf{s}, \mathbf{s}')$. Further, an analytic expression for the effect of a variance of the ensemble average on the solution of the CTRW transport equation is derived.

DOI: [10.1103/PhysRevE.81.031102](https://doi.org/10.1103/PhysRevE.81.031102)

PACS number(s): 05.60.-k, 05.10.Gg, 87.10.Ed, 05.40.Fb

I. INTRODUCTION

The physical basis for a theoretical treatment of transport in disordered systems, in the presence of a system-wide force field $\mathcal{F}(\mathbf{x})$ or spatially varying flow field $\mathbf{v}(\mathbf{x})$, is examined in the framework of a continuous time random walk (CTRW). After reviewing the basis for this framework for statistically homogeneous systems and presenting examples of its modification introduced by different $\mathcal{F}(\mathbf{x})$, the main focus in this study is on particle migration in a flow field $\mathbf{v}(\mathbf{x})$ in a disordered system. A transport equation is developed and numerical solutions are considered in extensive detail for different permeability fields and boundary conditions. The nature of the solutions as a function of key transport parameters (e.g., a characteristic time t_c) is explored, and solutions are also compared to those of the advection-dispersion equation. One class of new results indicates particle mass accumulations as a consequence of internal interfaces between large scale heterogeneities.

The CTRW is a generalization of the familiar random walk with a random time t , drawn from a probability density function (pdf) $\psi(t)$ at each transition, instead of the step number functioning as a discrete time [1]. The CTRW, based on a joint pdf $\psi(\mathbf{s}, t)$, with \mathbf{s} the transition displacement, was applied subsequently to transport problems [2,3]. It was discovered that if $\psi(\mathbf{s}, t)$ contains a sufficient time span of power-law time dependence (i.e., $\psi \sim t^{-1-\beta}$ with $0 < \beta < 2$) then there is a time window of anomalous transport [4,5] which has been observed in a wide range of media. In many studies it was shown that the power-law behavior derives from highly disordered systems; it is a signature feature, with which the CTRW has successfully accounted for a host of

measurements in these systems. In recent years the CTRW approach has been applied to tracer transport in saturated porous media to reproduce anomalous tracer plume propagation and breakthrough measurements in field and laboratory experiments [6–12]. In the latter the overall flow field can be assumed to be constant, while the distribution of local velocities (due to small-scale heterogeneities) is incorporated in $\psi(\mathbf{s}, t)$.

The derivation of CTRW from the standard transport equations describing the kinetics of realizations of physical systems has been considered in the literature [9]. The derivation is based on the ensemble average of these realizations, which results in the point-to-point fluctuations of the physical system described by $\psi(\mathbf{s}, t)$ in a homogeneous system. However, with an extended force field $\mathcal{F}(\mathbf{x})$ or a velocity field $\mathbf{v}(\mathbf{x})$, due to system-sized heterogeneities, the reduction to a homogeneous system must be modified significantly. The structure of the CTRW transport equations and e.g., the fractional advective-dispersive equation (FADE), which is a special limit case of CTRW, must be changed to accommodate $\mathbf{v}(\mathbf{x})$, $\mathcal{F}(\mathbf{x})$, large variances of system realizations and possibly chemical reactions. The case of $\mathcal{F}(\mathbf{x})$ is of particular relevance to the entire issue of whether forms of the fractional Fokker-Planck equation [13,14] accommodate this structural change.

In order to show how spatial inhomogeneity introduced by $\mathcal{F}(\mathbf{x})$ or $\mathbf{v}(\mathbf{x})$ modifies the physical basis for the CTRW model and related fractional derivative equations (e.g., FADE, fractional Fokker-Planck equation), we review in Sec. II the derivation of CTRW (and hence FADE) with a particular emphasis on the relation of $\psi(\mathbf{s}, t)$ to the transition rates of the physical system and the ensemble average of the system. We discuss cases in which the transition rates are

affected by an external potential. In this context the fractional Fokker-Planck equation is discussed. In Sec. III we develop the CTRW for a flow field $\mathbf{v}(\mathbf{x})$ in considerable detail by reducing the ensemble average to local regions of subsystem-sized heterogeneities and accounting for the laminar Darcy velocity field $\mathbf{v}(\mathbf{x})$ on the system scale, i.e., by using a position-dependent pdf $\psi(\mathbf{s}, t; \mathbf{x})$ which gives rise to the memory function $M(t; \mathbf{x})$. In Sec. IV the transport equation, incorporating $M(t; \mathbf{x})$ convoluted with the advection-dispersion operator, is solved numerically for both uniform and composite media. Our computational analysis remains on a scale that allows comparison to data available from laboratory experiments. In Sec. V an analytic expression of the effect of a variance of the ensemble average on the solution of the CTRW transport equation is derived.

II. DERIVATION OF BASIC EQUATIONS

Section II covers a number of topics related to the physical origin of the CTRW framework for transport based on the ensemble average of the Master Equation. In Sec. II A we review this derivation and in Sec. II B we review the calculation of $\psi(\mathbf{s}, t)$ based on an exact ensemble average of a physical model. In Secs. II C and II D we consider how the influence of $\mathbf{v}(\mathbf{x})$ and $\mathcal{F}(\mathbf{x})$ on the transition rates of the disordered system, respectively, affect FADE and the fractional Fokker-Planck equation.

We consider a class of phenomena that can be described by the probability density $c(\mathbf{s}, t)$ that a particle can be found at \mathbf{s} at time t if it was at \mathbf{s}_0 at $t=0$. This class excludes phenomena sensitive to wave function phase differences (e.g., [15]). A standard transport equation for $c(\mathbf{s}, t)$ is the Master Equation

$$\frac{\partial c(\mathbf{s}, t)}{\partial t} = - \sum_{\mathbf{s}'} w(\mathbf{s}', \mathbf{s}) c(\mathbf{s}, t) + \sum_{\mathbf{s}'} w(\mathbf{s}, \mathbf{s}') c(\mathbf{s}', t), \quad (1)$$

where $w(\mathbf{s}, \mathbf{s}')$ is the transition rate from \mathbf{s}' to \mathbf{s} ; the dimension of $\sum_{\mathbf{s}'} w$ is a function only of reciprocal time. The Master Equation holds for a specific realization of the system where the transition rates w depend on the position \mathbf{s} because the local site configurations vary.

A. Master equation as a random walk

The derivation of the relation between Eq. (1) and the CTRW starts with realizing that Eq. (1) describes a RW with a position-dependent transition pdf $\psi_{\mathbf{s}' \rightarrow \mathbf{s}}(\mathbf{s}, t)$ (in this notation \mathbf{s} denotes the position and $\mathbf{s}' - \mathbf{s}$ the displacement of the transition). The general equation for the random walker in this system, which is inhomogeneous in space and stationary in time, is

$$\mathcal{R}(\mathbf{s}, t) = \sum_{\mathbf{s}'} \int_0^t \psi_{\mathbf{s} \rightarrow \mathbf{s}'}(\mathbf{s}, t-t') \mathcal{R}(\mathbf{s}', t') dt', \quad (2)$$

where $\mathcal{R}(\mathbf{s}, t)$ is the probability density for a particle to just arrive at \mathbf{s} . The $\mathcal{R}(\mathbf{s}, t)$ depends on a specific configuration of the set of w in Eq. (1). The correspondence between the master equation and the random walk is

$$c(\mathbf{s}, t) = \int_0^t \Psi_{\mathbf{s}}(t-t') \mathcal{R}(\mathbf{s}, t') dt', \quad (3)$$

$$\Psi_{\mathbf{s}}(t) = 1 - \int_0^t \psi_{\mathbf{s}}(t') dt', \quad \psi_{\mathbf{s}}(t) \equiv \sum_{\mathbf{s}'} \psi_{\mathbf{s}' \rightarrow \mathbf{s}}(\mathbf{s}, t). \quad (4)$$

It is shown in Appendix B of [9] that there is an exact equivalence between Eq. (1) and Eqs. (2)–(4) with

$$\psi_{\mathbf{s}' \rightarrow \mathbf{s}}(\mathbf{s}, t) = w(\mathbf{s}', \mathbf{s}) \exp \left[-t \sum_{\mathbf{s}''} w(\mathbf{s}'', \mathbf{s}) \right]. \quad (5)$$

We emphasize that Eq. (5) is a site-dependent distribution of transitions of time and displacement coupled through the $w(\mathbf{s}', \mathbf{s})$.

The ensemble average of Eq. (5) over all the configurations of $w(\mathbf{s}', \mathbf{s})$ is the joint distribution $\psi(\mathbf{s}, t)$. To complete the derivation of the CTRW the next step is the evaluation of the ensemble average of Eq. (2), which involves the ensemble average of the product $\psi_{\mathbf{s}' \rightarrow \mathbf{s}}(t-t') \mathcal{R}(\mathbf{s}', t')$. To obtain an equation purely for the ensemble average of $\mathcal{R}(\mathbf{s}, t)$ we make the basic physical assumption that the ensemble average of the product is well approximated by the product of the ensemble averages, $\psi(\mathbf{s} - \mathbf{s}', t-t') \langle \mathcal{R}(\mathbf{s}', t') \rangle$, where $\langle \dots \rangle$ denotes the ensemble average. One form of correction to this “mean field” type of assumption will be considered in Sec. V. The CTRW equation is

$$R(\mathbf{s}, t) = \sum_{\mathbf{s}'} \int_0^t \psi(\mathbf{s} - \mathbf{s}', t-t') R(\mathbf{s}', t') dt', \quad (6)$$

where $R(\mathbf{s}, t) \equiv \langle \mathcal{R}(\mathbf{s}, t) \rangle$; Eq. (6) can be written in an equivalent form as a Generalized master equation (2), (4)–(7) of [9]. This generalized master equation is subsequently transformed via a Taylor expansion {Eq. (23) of [9]} into a second-order integrodifferential equation {Eq. (35) in [9]}:

$$\frac{\partial c(\mathbf{s}, t)}{\partial t} = - \int_0^t M(t-t') [\mathbf{v}_{\psi} \cdot \nabla c(\mathbf{s}, t') - \mathbf{D}_{\psi} : \nabla \nabla c(\mathbf{s}, t')] dt' \quad (7)$$

using the decoupled form $\psi(\mathbf{s}, t) = p(\mathbf{s}) \psi(t)$ and where the Laplace Transform (\mathcal{L}) of $M(t)$ is

$$\tilde{M}(u) \equiv t_c u \frac{\tilde{\psi}(u)}{1 - \tilde{\psi}(u)}, \quad (8)$$

where u is the Laplace variable, t_c is a characteristic time (cf. Sec. III) and \mathbf{v}_{ψ} , \mathbf{D}_{ψ} are the average particle velocity and dispersion, respectively (see Eqs. (30a) and (30b) in [9] for further explanation). Note that an approach to the derivation of a formal structure of a generalized master equation and the ensemble average of the master equation is carried out in [16].

B. Random site example

In general it is very difficult to characterize the transition rates $w(\mathbf{s}, \mathbf{s}')$ and carry out this ensemble average. For our

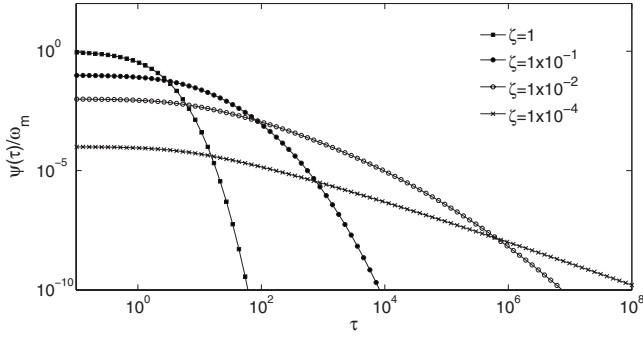


FIG. 1. Evolution of the dimensionless transition probability $\psi(\tau)/w_m$ Eq. (14) vs dimensionless time $w_m \tau$ for different values of the ζ parameter (after [17]).

present purpose, to evaluate the ensemble average of $\psi_{s'-s,s}(t)$ for a disordered system, it suffices to consider $\psi_s(t)$ in Eq. (4),

$$\psi_s(t) = \sum_{s'} w(s',s) \exp\left(-t \sum_{s'} w(s',s)\right) = -\frac{dQ_s}{dt} \quad (9)$$

(the sums are over $\Delta s' \equiv s' - s$, which we translate to be over s') where

$$Q_s \equiv \exp\left(-t \sum_{s'} w(s',s)\right) \quad (10)$$

and

$$\psi(t) = -\frac{d}{dt} \langle Q_s \rangle. \quad (11)$$

The $\psi(t)$ is an excellent measure of the spectrum of transition times in a system with spatially compact transition rates.

The calculation of $\psi(t)$ or $\langle Q_s \rangle$ for the case of a configuration of random spatial locations or sites, between which there are the transitions $w(s',s) = w(s' - s)$, can be carried out exactly [3],

$$\langle Q_s \rangle = \exp\left(-N_\zeta \int d^3x \{1 - \exp[-w(\mathbf{x})t]\}\right) \quad (12)$$

where N_ζ is the site density. To evaluate Eq. (12) further we choose a standard transition rate between local sites,

$$w(s' - s) = w_m \exp(-|s' - s|/r_o), \quad (13)$$

where r_o is the range of the transitions and w_m is the maximum rate. Substituting Eq. (13) into Eq. (12) and then Eq. (11), we derive [17],

$$\frac{\psi(\tau)}{w_m} = \zeta_3 F_3 \left[\begin{matrix} 1, 1, 1 \\ 2, 2, 2 \end{matrix} ; -\tau \right] e^{-\zeta_4 F_4 \left[\begin{matrix} 1, 1, 1, 1 \\ 2, 2, 2, 2 \end{matrix} ; -\tau \right]}, \quad (14)$$

where $\tau \equiv w_m t$, $\zeta \equiv 4\pi N_\zeta r_o^3$, and ${}_p F_q$ is the generalized hypergeometric function as defined in [18].

In Fig. 1 many of the generic features of the spectrum of transition times for a disordered system can be seen. The parameter ζ can be written as $\zeta = 3(r_o/r_N)^3$ and for $r_o \ll r_N$ the rates are sensitive to the separations between sites and hence

generate a wide range of rates, i.e., for the lower values of ζ , $\psi(\tau)$ is wider and varies slowly. There are large ranges of τ where $\psi(\tau)$ varies approximately as a power law $\sim \tau^{-1-\beta}$ and β can have a value between 0 and 2. It is this power-law behavior of $\psi(\tau)$ that can generate anomalous (or non-Fickian) transport within the context of the CTRW transport model. Corresponding to each value of ζ there is a ‘‘cutoff’’ τ_c where $\psi(\tau)$ decays faster than $\sim \tau^{-3}$ for $\tau > \tau_c$. This is a region where there is a transition to normal (Fickian) transport. The parameter ζ can be seen to be a measure of the disorder in the system; there is clearly an interplay between the degree of disorder, the power-law region and the ‘‘cutoff’’ region. These are general features for large τ that persist for $\psi(\tau)$ for the disordered systems so far encountered (including particles borne by complex flow fields). The small τ region can be important for the coupled $\psi(s,t)$ if the dependence on the displacement s is slowly varying, i.e., a power law [19]. For a compact spatial dependence, as in the example above, the uncoupled approximation $\psi(s,t) = p(s)\psi(t)$ is effective [19].

C. Connection to the fractional advective-dispersion equation

The representation of $\psi(\tau) \sim \tau^{-1-\beta}$ for $\tau \gg 1$ (with no cutoff) and for $\beta < 1$ corresponds to a FADE formulation, which is a limit subset of CTRW. The temporal FADE can be written as [20]

$$\frac{\partial c(\mathbf{x},t)}{\partial t} = -\frac{\partial^{1-\beta}}{\partial t^{1-\beta}} \{ \mathbf{v}^*(\mathbf{x}) \cdot \nabla c(\mathbf{x},t) - \nabla \cdot [\mathbf{D}^*(\mathbf{x}) \cdot \nabla c(\mathbf{x},t)] \}, \quad (15)$$

with the definition of the operator

$$\frac{\partial^{-\gamma}}{\partial t^{-\gamma}} c(x,t) \equiv \frac{1}{\Gamma(\gamma)} \int_0^t dt' \frac{c(x,t')}{(t-t')^{1-\gamma}}. \quad (16)$$

In Eq. (15) the asterisks on \mathbf{v}^* , \mathbf{D}^* indicate that these quantities do not have the same dimensions as usual, i.e., \mathbf{v}^* has dimensions $[L]/[t^\beta]$. The form of Eq. (15), as we will discuss in this subsection and in Sec. III, is a result of decoupling the interaction between the system-wide $\mathbf{v}(\mathbf{x})$ and the underlying transition rates $w(s',s)$.

The complete derivation of the equivalence of the FADE and the pure power-law $\psi(\tau)$ case of CTRW is found in [9,21]. Therefore the physical basis for the temporal FADE is the same as the CTRW—an ensemble average of a standard transport equation (e.g., the master equation) over realizations of a disordered system where statistical homogeneity is valid. In the case of the Fokker-Planck equation [22], a similar structure as Eq. (15) has appeared for the fractional derivative form; using the notation of [13,14,23], the one-dimensional form is

$$\frac{\partial W}{\partial t} = \frac{\partial^{1-\beta}}{\partial t^{1-\beta}} \left[\frac{\partial V'(x)}{\partial x} \frac{1}{m \eta_\beta} + K_\beta \frac{\partial^2}{\partial x^2} \right] W(x,t), \quad (17)$$

where K_β is a generalized diffusion constant, m a mass, η_β is a generalized friction coefficient, $V(x)$ is an external potential and $\mathcal{F}(x) = -\partial V(x)/\partial x \equiv -V'(x)$.

D. Potentials, transition rates and the fractional Fokker-Planck equation

The fractional Fokker-Planck equation (Sec. II D) [13,14] contains an applied force field $\mathcal{F}(\mathbf{x})$. The basic enquiry now is: how does the application of $\mathcal{F}(\mathbf{x})$ to a disordered system affect the derivation of the fractional Fokker-Planck equation. The answer depends on how the $\mathcal{F}(\mathbf{x})$ affects the rates $w(\mathbf{s}', \mathbf{s})$ in Eq. (1). We will consider a number of examples: (i) the direct application of a force field to Eq. (1) for a specific realization, (ii) the effect of a constant electric field on the ensemble average of Eq. (5), and (iii) the change in fluid flow in a permeability field.

The influence of a force field on the form of Eq. (1) occurs exclusively through its effect on the transition rates $w(\mathbf{s}', \mathbf{s})$. In (24) and (25) the master equation (1) was solved directly, numerically, in a specific realization of a doped molecular crystal. The (activated) transport of electrons via molecular polaron transition rates between sites was calculated in the presence of a combined constant electric field and Coulomb potential. The transition rates depend on the molecular energy level difference $\Delta\epsilon$ between the sites, while $\Delta\epsilon(\mathbf{s})$ varies with position \mathbf{s} in the Coulomb well. The $\Delta\epsilon$ due to the electric field is not \mathbf{s} dependent, in the ordered case, as the spatial displacement of each transition is constrained to the nearest neighbor in the crystal. Hence, Eq. (5) as determined in [24,25] is a function of \mathbf{s} in the Coulomb part of the potential. A \mathbf{s} dependence due to the Coulomb potential persists if the molecular system is disordered, therefore the ensemble average of Eq. (5) will retain its \mathbf{s} dependence and the ensemble average of system will be inhomogeneous in space; as a consequence, one must use the hybrid approach in [26] and Sec. III. An inhomogeneous ensemble average is incompatible with the fractional Fokker-Planck equation (Sec. II D), which requires a β in the fractional derivative (16) independent of $\mathcal{F}(\mathbf{x})$, i.e., a constant β .

We next consider the effect of a potential on the ensemble average of Eq. (5) [27,28]. The system is the same as that in [3]. Here, we modify the transition rate [Eq. (13)] by the addition of $e\mathbf{E}\cdot(\mathbf{s}-\mathbf{s}')/k_B T$ to the exponent, where \mathbf{E} is a constant electric field and k_B is Boltzmann's constant. In this case the displacement $\mathbf{s}-\mathbf{s}'$ varies from site to site, hence the spectrum of rates is \mathbf{E} dependent [28], $\psi_E(t)$, but the ensemble average is still homogeneous. The common approximation to $\ln \psi(t)/\ln t$ over a large time interval is $-1-\beta$; in this case we have a $\beta(E)$ in $\psi_E(t)$ [27,28]. Thus, for a simple applied potential one cannot use a constant β in the fractional Fokker-Planck equation.

In experiments of fluid flow in saturated porous media [29], the fit using $\psi(t) \sim t^{-1-\beta}$ to the breakthrough curves of concentration vs time, corresponding to different flow velocities v , necessitated the use of a v -dependent β . This was shown to be an artifact of not using the full functional form of $\psi(t)$, which was represented by a truncated power law (TPL, see Sec. III), i.e., a cutoff to the power-law time regime. In [30] the complete set of the breakthrough curve data was fit with one TPL with fixed β for all the values of v . In this case changing v did not change the rate spectrum (the streamlines do not change) but instead shifted the observation window along the time axis. Again this change in the

applied $\mathcal{F}(\mathbf{x})$ of a pressure gradient points out the two problems with the fractional Fokker-Planck equation outlined in the previous two paragraphs, namely, the inappropriateness of a constant β and the limitation of using $\ln \psi(t)/\ln t \approx -1-\beta$.

In summary, we emphasize there is no universality: each problem of transport involving an external potential applied to a disordered system must be analyzed individually. However, in general the potential affects the transition rates and use of the master equation (1) as the physical basis for the ensemble averaged transport equations is incompatible with the independence of the fractional derivative and the nature of $\mathcal{F}(\mathbf{x})$. In Sec. III we consider one approach to incorporate the inhomogeneity of the spectrum of transition rates into the transport equation.

III. TRANSPORT IN A SPATIALLY NON-UNIFORM FLOW FIELD

The goal is to develop a prototype transport equation for a system with statistical inhomogeneity. The basic idea is to determine the ensemble average in local regions, i.e., due to small scale heterogeneities, and solve on the larger scale the pde version of the CTRW for this inhomogeneous system [26] (a fractional derivative diffusion equation formulation for this system is studied in [31]). We consider the case of fluid flow and solute transport in saturated porous media. The laminar Darcy flow is $\mathbf{q}(\mathbf{x})$ with velocity $\mathbf{v}(\mathbf{x})=\mathbf{q}/n$ and porosity n . In this macroscopic velocity field the $\psi(\mathbf{s}, t)$ is chosen to be position dependent,

$$\psi(\mathbf{s}, t; \mathbf{x}) = p(\mathbf{s}; \mathbf{x})\psi(t; \mathbf{x}), \quad (18)$$

where \mathbf{x} denotes the spatial position and \mathbf{s} is the displacement of the transition. We use the approximate decoupled form of $\psi(\mathbf{s}, t)$ (for an appraisal of this approximation see [19]). We consider a two-dimensional, isotropic medium with dispersivity matrix $\underline{\alpha}$ having diagonal entries α_x and α_y (as subscripts x, y refer to the components along the x, y axis). The transition probability in space $p(\mathbf{s}; \mathbf{x})$ is chosen to be a product of Gaussians, $\mathcal{N}(\mu, \sigma)$, in s_x and s_y ,

$$p(\mathbf{s}; \mathbf{x}) = \mathcal{N}[v_x(\mathbf{x})t_c, \sqrt{\alpha_x(\mathbf{x})|\mathbf{v}(\mathbf{x})|}t_c] \mathcal{N}[v_y(\mathbf{x})t_c, \sqrt{\alpha_y(\mathbf{x})|\mathbf{v}(\mathbf{x})|}t_c], \quad (19)$$

where t_c is some characteristic time whose role will be discussed in detail later. Some of the applications we consider will involve a space-dependent $t_c(\mathbf{x})$. The transition probability in time $\psi(t; \mathbf{x})$ is chosen to be a truncated power law (TPL). The TPL captures the main features of Fig. 1 with three parameters

$$\psi(t; \mathbf{x}) = N \frac{e^{-t/t_2}}{t_1 \left(1 + \frac{t}{t_1}\right)^{1+\beta}}, \quad (20)$$

with the normalization constant $N = \left[\left(\frac{t_1}{t_2}\right)^\beta e^{t_1/t_2} \Gamma(-\beta, \frac{t_1}{t_2})\right]^{-1}$, where $\Gamma(a, x)$ is the incomplete Gamma function [18]. The parameter t_1 is a scaling time, t_2 is a cutoff time of the power-law region and β controls this region $t_1 < t < t_2$; any of these parameters can be \mathbf{x} dependent.

In [21] the general advection-dispersion equation (ADE) with \mathbf{x} -dependent velocity $\mathbf{v}(\mathbf{x})$ and dispersion $\mathbf{D}(\mathbf{x})$ was derived from the master equation [Eq. (14) of [21]], for a specific realization. To incorporate local stochastic effects in this equation, as discussed above, we generalize the velocity and dispersion as in Eq. (7) to include the memory term $M(t; \mathbf{x})$ [recall Eq. (8)], which is now \mathbf{x} dependent; its \mathcal{L} form is

$$\tilde{M}(u; \mathbf{x}) = \frac{t_c u \tilde{\psi}(u; \mathbf{x})}{1 - \tilde{\psi}(u; \mathbf{x})}. \quad (21)$$

In deriving this result we begin again with the \mathcal{L} form of the generalized master equation [9,21].

$$u \tilde{P}(\mathbf{x}, u) - P(\mathbf{x}, 0) = \int \phi(\mathbf{x} - \mathbf{x}', u; \mathbf{x}') \tilde{P}(\mathbf{x}', u) d\mathbf{x}' - \int \phi(\mathbf{x}' - \mathbf{x}, u; \mathbf{x}) \tilde{P}(\mathbf{x}, u) d\mathbf{x}', \quad (22)$$

where

$$\phi(\mathbf{x}' - \mathbf{x}, u; \mathbf{x}) = \frac{p(\mathbf{x}' - \mathbf{x}; \mathbf{x})}{t_c} \tilde{M}(u; \mathbf{x}) \quad (23)$$

and $P(\mathbf{x}, t)$ is a normalized concentration or probability. The function $\phi(\mathbf{x} - \mathbf{x}', u; \mathbf{x}') \tilde{P}(\mathbf{x}', u)$ is expanded in the \mathbf{x}' variable about \mathbf{x} similar to Eq. (6) of [21]. The zeroth-order term vanishes with the second integral on the right side of Eq. (22) [after integrating $p(\mathbf{x}' - \mathbf{x}; \mathbf{x})$]. We obtain [32]

$$u \tilde{P}(\mathbf{x}, u) - P(\mathbf{x}, 0) = -\nabla \left[\tilde{M}(u; \mathbf{x}) \frac{\mu}{t_c} \tilde{P}(\mathbf{x}, u) \right] + \nabla \left\{ \nabla \left[\tilde{M}(u; \mathbf{x}) \frac{\sigma^2}{t_c} \tilde{P}(\mathbf{x}, u) \right] \right\} \quad (24)$$

because higher order moments are zero for the Gaussian distribution in Eq. (19). By choosing $\mu = t_c \mathbf{v}$ and $\sigma^2 = t_c |\mathbf{v}| \alpha$, with α the isotropic dispersivity matrix having diagonal entries α_x and α_y , we obtain the integropartial differential equation

$$n(\mathbf{x}) \frac{\partial c(\mathbf{x}, t)}{\partial t} = -\nabla \int_0^t \{ M(t-t'; \mathbf{x}) \mathbf{q}(\mathbf{x}) c(\mathbf{x}, t') - \nabla [\mathbf{q}(\mathbf{x}) | \alpha(\mathbf{x}) M(t-t'; \mathbf{x}) c(\mathbf{x}, t')] \} dt' \quad (25)$$

with $n(\mathbf{x}) c(\mathbf{x}, t) \equiv P(\mathbf{x}, t)$. Note that for the memory function $M(t-t'; \mathbf{x}) = \delta(t-t')$, the equation reduces to the ADE.

In contrast to a previous analysis [26], we do not neglect first-order derivatives of $M(t; \mathbf{x})$, so that the pdf is fully in mass conservative form. We demonstrate in the next section that including first-order derivatives has important consequences for the steady-state solution of the pdf. We solve Eq. (25) neglecting the second order derivatives of $M(t; \mathbf{x})$, α and \mathbf{q} .

A. Numerical methods

We can consider two approaches to solving the transport problem in the flow field $\mathbf{v}(\mathbf{x})$. One consists of solving nu-

merically an integropartial differential equation such as Eq. (25) [26,33] and the other is to implement particle tracking in which each particle is advanced in time and space by choosing \mathbf{s} and t from the distribution $\psi(\mathbf{s}, t)$ [19,34]. Both approaches have advantages and disadvantages. Solving the differential equation requires a stable algorithm for numerical Laplace transform inversion \mathcal{L}^{-1} . For particle tracking, interpolation of the velocity field performed at each particle transit slows the simulation process significantly. In addition the number of particles required to achieve sufficient statistics increases for long-tailed waiting time distributions. Note that because we neglect second-order derivatives of $M(t; \mathbf{x})$, α and \mathbf{q} , these two methods are only strictly equal in the case of space-independent $M(t; \mathbf{x})$, α , and a divergence-free flow field \mathbf{q} .

We focus here on the differential equation approach. We used a vertex-centered finite volume scheme in MATLAB[®] on an equally spaced rectangular grid to solve both the flow and transport equations. The steady-state Darcy flow field $\mathbf{q}(\mathbf{x})$ is calculated by solving the Poisson equation for the pressure head $h(\mathbf{x})$,

$$\frac{\partial}{\partial x} K_x \frac{\partial h(\mathbf{x})}{\partial x} + \frac{\partial}{\partial y} K_y \frac{\partial h(\mathbf{x})}{\partial y} = 0. \quad (26)$$

Because the medium is assumed to be isotropic, the hydraulic conductivity matrix \mathbf{K} is diagonal with entries K_x and K_y . The flow field is then given by

$$\mathbf{q}(\mathbf{x}) = -\mathbf{K} \cdot \nabla h(\mathbf{x}), \quad (27)$$

whose solution is used to solve the transport Eq. (25) in Laplace space. To minimize classical numerical dispersion, the grid spacing d_g was chosen to be slightly less than twice the smallest dispersivity, i.e., $d_g = 0.1 \text{ cm} < 0.1064 \text{ cm}$ [35]. Discontinuities in the parameter values at the interfaces between different types of porous medium were linearly interpolated on the next nearest grid lines to the interface. The \mathcal{L}^{-1} algorithm of de Hoog *et al.* [36] was employed to invert the numerical solution $\tilde{c}(\mathbf{x}, u)$, as used in the publicly available CTRW MATLAB[®] TOOLBOX [37].

To confirm that the numerical solution method was correct, four independent tests were performed. First we ensured that the results for transport in a uniform, one-dimensional column matched the semianalytical solutions (using the CTRW Toolbox [37]). Second we confirmed that the mass fluxes into and out of the domain were equal for a uniform regime at long times. Third we compared breakthrough curves to the results of a particle tracking run for a two-dimensional uniform medium with a nonuniform flow field and the CTRW parameter set $\beta = 1.65$, $t_c = t_1 = 1 \text{ s}$, $t_2 = 10^6 \text{ s}$, obtaining similar results. Fourth we matched the solution for a uniform medium, using a memory function equal to unity (i.e., assuming Fickian, advective-dispersive transport behavior), against the results obtained from an independently written finite element code.

B. Characteristic time t_c

The CTRW transport equation (25) is a nonlocal-in-time equation. Hence, the concentration profile at time t , in con-

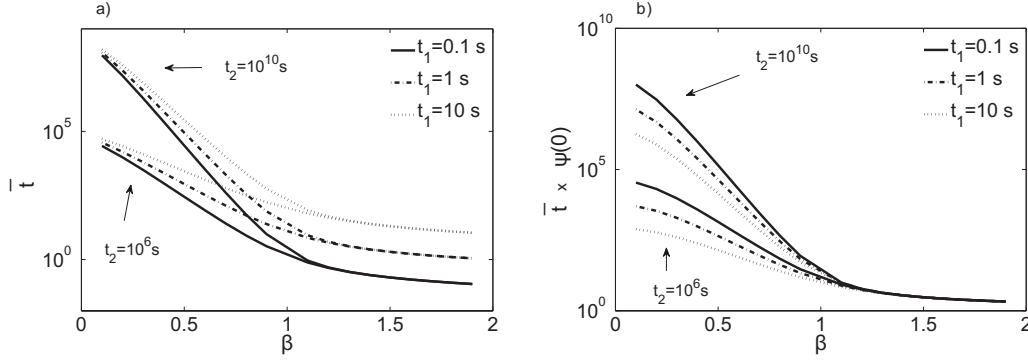


FIG. 2. (a) Mean transit time \bar{t} (s) vs β (dimensionless) for different values of t_1 and t_2 . (b) Limit value for $\tilde{M}(u)$ (dimensionless) in the case where the absolute value of the complex argument u goes to infinity [$\lim_{|u| \rightarrow \infty} \tilde{M}(u) = \bar{t}\psi(t=0)$] for different values of t_1 and t_2 .

trast to transport described by the ADE, has contributions from earlier times. This behavior originates from the broad distribution of transit times due to local heterogeneity and is described by the power-law tail of $\psi(s; \mathbf{x})$. The memory function $M(t; \mathbf{x})$ contains the $\psi(s; \mathbf{x})$ and constitutes the heart of the CTRW approach. The $M(t; \mathbf{x})$ includes a characteristic time parameter t_c whose physical motivation and impact on the final solution will be discussed in this section.

We examine the steady-state solution $\partial c(\mathbf{x}, t) / \partial t = 0$ of Eq. (25) given a step input at the inlet and using Eq. (20). Because

$$\lim_{u \rightarrow 0} \tilde{M}(u; \mathbf{x}) = \frac{t_c(\mathbf{x})}{\bar{t}(\mathbf{x})} \quad \text{with} \quad \bar{t} = \int_0^{\infty} t \psi(t; \mathbf{x}) dt = N t_2 - (t_1 + \beta t_2) \quad (28)$$

we see that the steady-state concentration profile $c_s(\mathbf{x}) = \lim_{t \rightarrow \infty} c(\mathbf{x}, t) = \lim_{u \rightarrow 0} u \tilde{c}(\mathbf{x}, u)$ is a solution of the partial differential equation

$$\nabla \left[\frac{t_c(\mathbf{x})}{\bar{t}(\mathbf{x})} \mathbf{q}(\mathbf{x}) c_s(\mathbf{x}) - \frac{t_c(\mathbf{x})}{\bar{t}(\mathbf{x})} |\mathbf{q}(\mathbf{x})| \alpha(\mathbf{x}) \nabla c_s(\mathbf{x}) \right] = 0. \quad (29)$$

Now, increasing the residence time in any physical system promotes a transition from non-Fickian to Fickian behavior. Therefore one expects the concentration profile at long times to be constant, given a step input at the inlet; no other result can be supported experimentally.

If the memory function (21) is not space dependent, meaning that its parameters β , t_1 , and t_2 are not space dependent, then from Eq. (29) we see that the steady-state concentration profile for a step input at the inlet is, as expected experimentally, constant for either of the two possible choices for the characteristic time t_c , namely the scaling time t_1 of the TPL or the mean time \bar{t} of the TPL. The memory function can be taken to be space independent in a system whose heterogeneities are on a scale much smaller than the overall size of the system.

For a domain composed of patches of uniform media with different properties (see Sec. IV B, Setups S3 and S4) where the sizes of the patches are of the order of the domain size,

we assign different transition time parameters to each patch. As a consequence the memory function becomes space dependent. But for a space-dependent memory function, it is seen from Eq. (29) that we must choose $t_c = \bar{t}$ to achieve the physically reasonable, constant steady-state concentration profile at long times.

The parameter t_c appears in both Eqs. (19) and (21). In Eq. (19) the relation $\bar{s} = t_c \mathbf{v}(\mathbf{x})$ between the mean transition distance, the velocity and the characteristic time appears. The quantity $|\bar{s}| = k_d d_p$ is a measure of the local spatial scale in the regions of heterogeneity that are considered probabilistically (where d_p is a grain size and k_d is a constant). In Fig. 2(a) we confirm that the mean $\bar{s} = \bar{t} \mathbf{v}(\mathbf{x})$ is of realistic size, by examining the dependence of \bar{t} on t_1 and β using Eq. (28). First we see from the graph that for $\beta > 1$, \bar{t} is dominated by t_1 , whereas for small values of β , \bar{t} is dominated by t_2 . For $\beta \rightarrow 2$ and $t_1 \ll t_2$ one can show from Eq. (28) that \bar{t} approaches t_1 . In our setups the maximal velocity in the system is at the inlet, which we chose to be of the order of 10^{-1} cm/s and smaller. In these cases we see that \bar{s} is of reasonable size for $\beta > 0.8$.

IV. NUMERICAL RESULTS

In the numerical solutions we consider a square domain (25×25 cm²) containing different arrangements of porous media (see Fig. 3). We use values of (isotropic, homogeneous) hydraulic conductivity K , grain diameter d and porosity n for two types of porous materials employed frequently in laboratory experiments examining solute transport in water saturated media: “coarse” quartz sand ($K=0.5$ cm/s, $d=1.105$ mm, $n=0.35$) and “medium” quartz sand ($K=0.15$ cm/s, $d=0.532$ mm, $n=0.3$) [29,38]. In the “set-ups” shown in all figures below, coarse and medium sands are represented by dark gray and light gray colors, respectively. In all cases, the dispersivity α is set equal to the grain size. For comparison to an experiment in a uniform porous medium, the domain thickness is 1.52 cm.

The full two-dimensional solutions for the ADE and for the integropartial differential equation (25) are presented for different domain structures and boundary conditions. The solutions to Eq. (25) are examined in the parameter space of the memory function (21). In general, the solutions exhibit

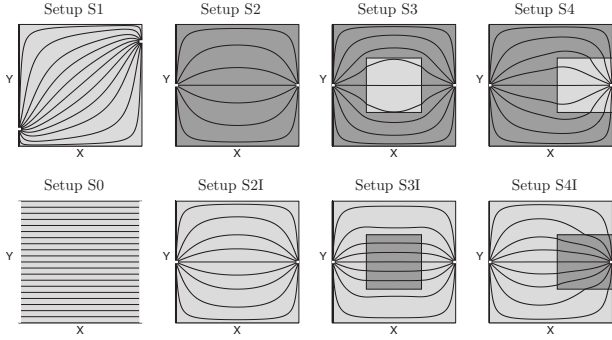


FIG. 3. Uniform (S0, S1, S2, S2I) and composite (S3, S3I, S4, S4I) media setups used for transport calculations. Streamlines are drawn in each image to illustrate the different flow fields. Light color denotes medium sand, while dark color denotes coarse sand. Inlet and outlet faces extend across the entire y axis for setup S0. In setup S1 the inlet extends from $(x,y)=(0,3.25)$ cm to $(0,3.75)$ cm and the outlet from $(25,21.25)$ cm to $(25,21.75)$ cm. In setups S2-S4 and S2I-S4I the inlet extends from $(x,y)=(0,12.25)$ cm to $(0,12.75)$ cm and the outlet from $(25,12.25)$ cm to $(25,12.75)$ cm. Unless otherwise specified, the boundary conditions are as follows. Flow boundary conditions: $\mathbf{q}_{\text{inlet}}=(0.044,0)$ cm/s (corresponding to a volumetric flow rate of $Q_{\text{in}}=2$ ml/min), $h_{\text{outlet}}=0$ and $\mathbf{q}=(0,0)$ otherwise. Transport boundary conditions: $c_{\text{inlet}}=1$ mol/cm², $\partial c_{\text{outlet}}/\partial x=0$ and $\mathbf{n}\cdot[\mathbf{q}c-\nabla(\mathbf{q}\alpha c)]=0$ otherwise (where \mathbf{n} is the normal to the boundary).

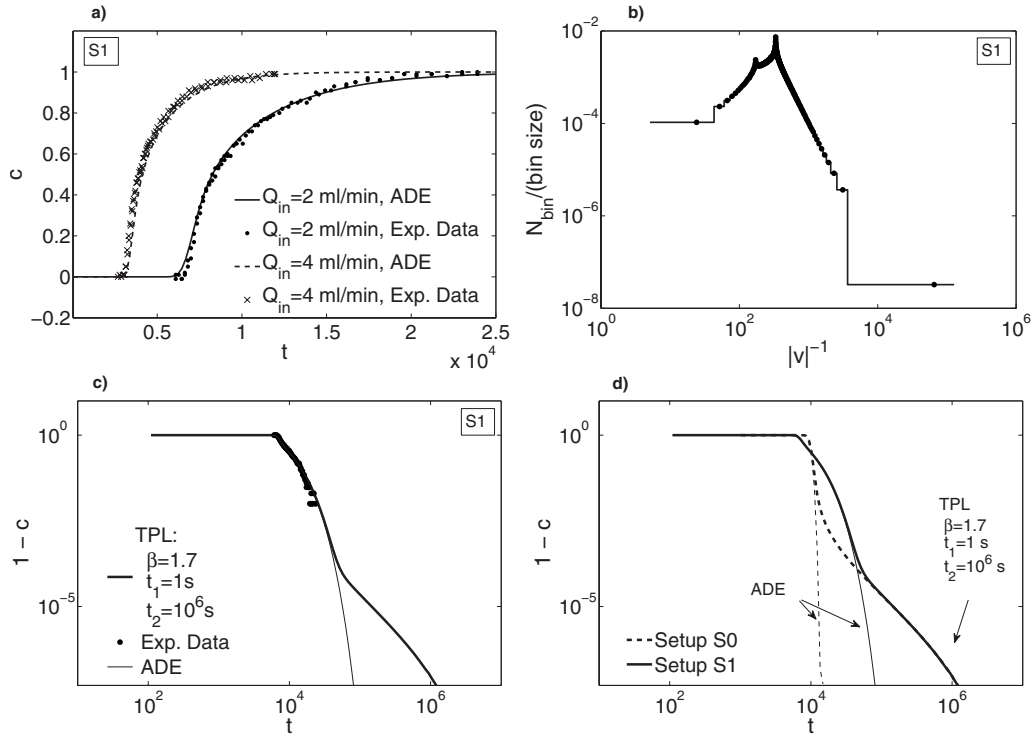


FIG. 4. Breakthrough curves [c (mol/cm²) vs t (s)] and velocity distribution [v (cm/s)] in a uniform medium with nonuniform flow field (Setup S1), showing comparisons to experimental results and to transport in a uniform flow field. (a) Comparison of the ADE solution in Setup S1 to measured breakthrough curves in laboratory experiments (denoted “Expt. Data”) with two different inlet flow rates. (b) Velocity distribution in Setup S1 for volumetric inlet flow rate $Q_{\text{in}}=2$ ml/min. Each horizontal segment in this step graph represents the velocity⁻¹ range (bin size) containing $N_{\text{bin}}=1000$ values from a total of 249 000 [which is the total number of grid nodes chosen to solve Eq. (20)]. The dots indicate the centers of each range, which do not appear to be centered in the graph because of the logarithmic scale. (c) Comparison between ADE and TPL fits to the laboratory measurements with $Q_{\text{in}}=2$ ml/min. (d) Comparison between breakthrough curves from TPL solutions for Setups S0 and S1 with $Q_{\text{in}}=2$ ml/min. The ADE solutions are included for comparison.

similarity to the ADE solution at short times and at asymptotically long times. This is a result of the shape of the memory function $\tilde{M}(u)$ (see Figs. 6 and 7 of [33]): The $\lim_{u \rightarrow 0} \tilde{M}(u) = \kappa_0$ where κ_0 is a constant and is equal to 1 for $t_c = \bar{t}$ and $\lim_{u \rightarrow \infty} \tilde{M}(u) = \kappa_\infty$ where κ_∞ is a constant and is equal to $\bar{t}\psi(0)$. For constant regions of $\tilde{M}(u)$ the solutions of Eq. (25) in the corresponding time regions are those of the ADE for a uniform medium. In Fig. 2(b) we plot $\bar{t}\psi(0)$ vs β for a range of t_1 and t_2 . We note that for $\beta > 1$ the value of $\bar{t}\psi(0)$ is independent of t_1 and t_2 , and varies very slowly with β . Hence the short time solutions of Eq. (25) are independent of t_1 and t_2 , as will be exhibited in some of the plots in Figs. 4 and 5.

The solutions of Eq. (25) are intended for comparison to transport in highly heterogeneous systems. However, as noted in Sec. I, laboratory experiments using various arrangements of uniform and heterogeneous porous media with statistical stationarity have exhibited non-Fickian transport. We refer here to domains with statistical homogeneity as “uniform” media, and heterogeneous domains consisting of a combination of large (relative to the domain size) porous media patches with different properties as “composite” media.

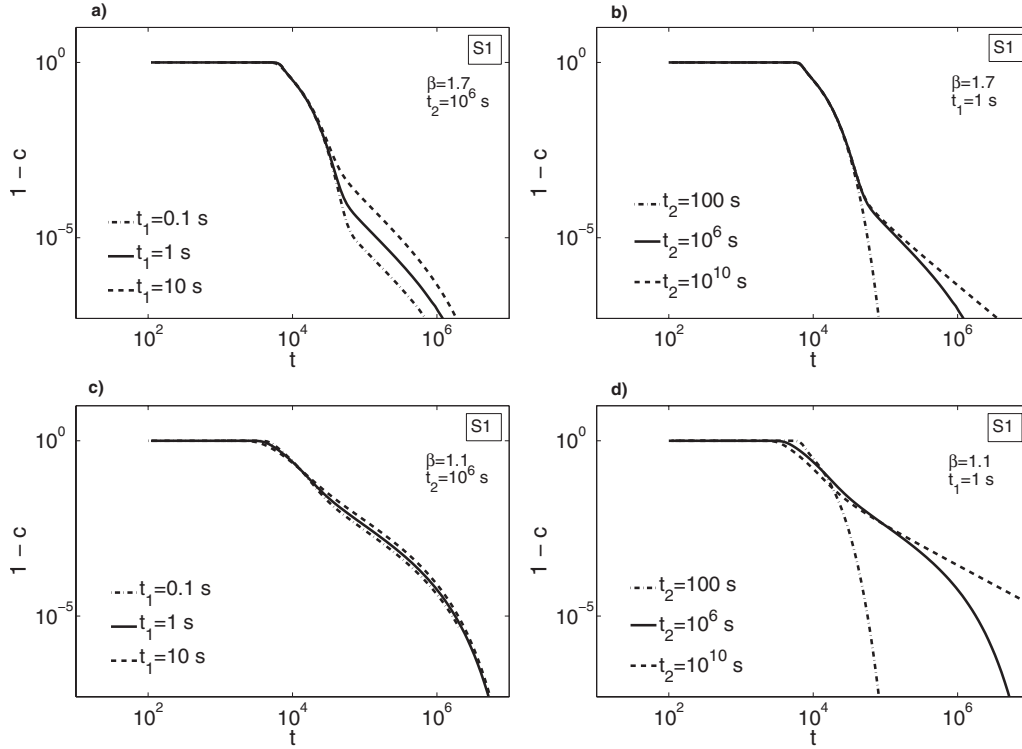


FIG. 5. Comparison of breakthrough curves [c (mol/cm²) vs t (s)] in a uniform medium (Setup S1) using the TPL solution, as a function of values of t_1 , t_2 , and β . (a) Effect of varying t_1 , for $\beta=1.7$, $t_2=10^6$ s. (b) Effect of varying t_2 , for $\beta=1.7$, $t_1=1$ s. (c) Effect of varying t_1 , for $\beta=1.1$, $t_2=10^6$ s. (d) Effect of varying t_2 , for $\beta=1.1$, $t_1=1$ s.

A. Uniform medium

We first consider setup S1 in Fig. 3, a domain containing homogeneous porous material. To test the numerical method we employ, we measured tracer transport in this domain in a laboratory experiment; breakthrough curves of chloride were determined at the outlet using electrical conductivity. For this case we consider a transition time distribution that is not position dependent. The inlet flow rates were $Q=2$ ml/min and $Q=4$ ml/min. The measured breakthrough curves were fit best by the ADE [see Fig. 4(a)]. From Fig. 4(c), it is seen that the breakthrough curves for the measured time period do not exhibit long tailing, although the velocity distribution [see Fig. 4(b)] is long tailed. However, the power-law slope of the $1/v$ plot [Fig. 4(b)] is -3 ; this value corresponds to a β of 2, which is a region of marginal Fickian behavior. As outlined in [39] long tailing in the velocity distribution can induce long tailing in the breakthrough curve. From Fig. 4(c), a CTRW solution with values of β close to Fickian is seen to first follow the ADE solution before showing tailing effects in a very low concentration, long time regime. Note that high-resolution measurements over such long times are difficult to obtain in laboratory experiments.

The behavior upon variation of any one of the parameters Q_{in} , β , t_1 , or t_2 is qualitatively the same in uniform media with uniform and nonuniform flow fields (setups S0 and S1, respectively). We therefore include only one comparison graph [Fig. 4(d)] from which the main differences can be read. The feature that distinguishes the uniform flow breakthrough curves from the nonuniform ones is the later initial

breakthrough time in the uniform flow field, even though the volumetric inlet flow rate is the same. However, once the initial breakthrough occurs, the concentration increases much faster than in the nonuniform flow case [Fig. 4(d)]. Both behaviors can be understood by recognizing that in the uniform flow a particle traverses each possible path with the same velocity whereas in nonuniform flow there exist paths with overall higher and lower velocities.

The differences in the breakthrough curves are now examined upon variation of the inlet flow rate and the parameters of the transit time distribution β , t_1 , and t_2 for the uniform medium with a nonuniform flow (setup S1). The reference parameter set, which is always represented by a solid line in Figs. 5 and 6, has values $Q_{in}=2$ ml/min, $\beta=1.1, 1.7$, $t_1=1$ s, and $t_2=10^6$ s for Fig. 5 and values $Q_{in}=2$ ml/min, $\beta=1.1, 1.9$, $t_1=1$ s and $t_2=10^{10}$ s for Fig. 6. Parameters are varied individually to examine their relative influence on the breakthrough curves.

The response of the breakthrough curves to a variation of t_1 is shown in Fig. 5(a) for $\beta=1.7$ and Fig. 5(c) for $\beta=1.1$. For a value of β close to Fickian transport, the parameter t_1 controls the concentration at which the breakthrough curve starts to deviate from the ADE solution and enter long tailing [Fig. 5(a)]. For smaller values of β [Fig. 5(c)], the breakthrough curve deviates considerably from the ADE solution. The breakthrough occurs earlier than in the ADE solution and displays long tailing. Therefore a change of t_1 in the range presented has practically no effect on the breakthrough curves for a low value of β . We note that for the case of a uniform medium, breakthrough curves with different t_1 can

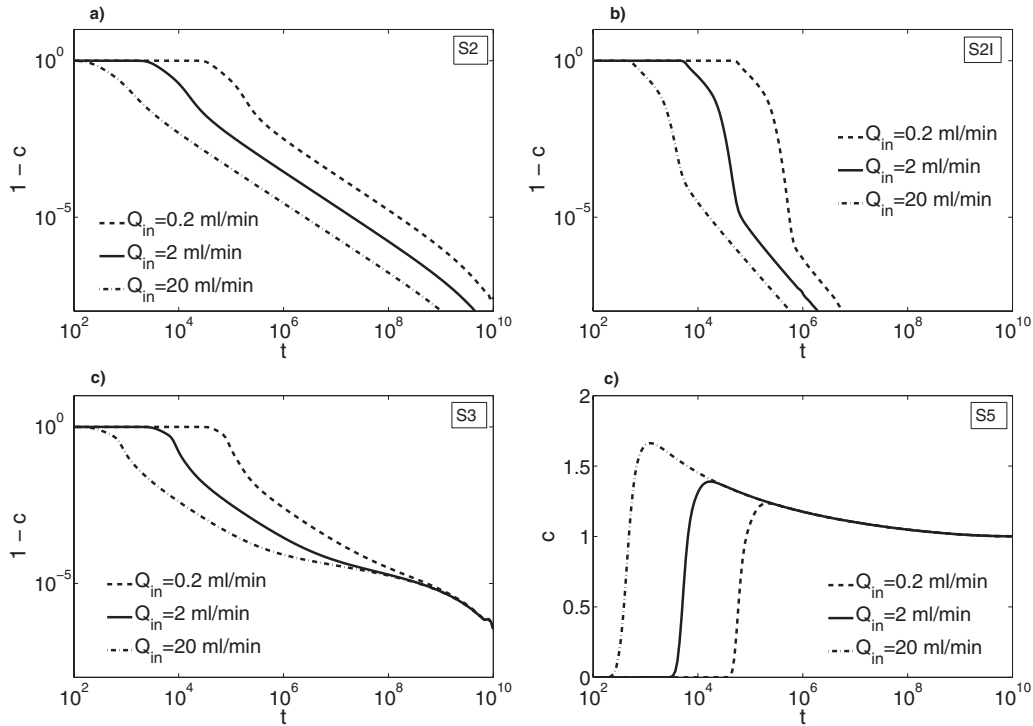


FIG. 6. Comparison of breakthrough curves [c (mol/cm²) vs t (s)] between uniform and composite media (recall Fig. 3) for different inlet flow rates Q_{in} . In all cases, $t_1=1$ s and $t_2=10^{10}$ s. Medium and coarse sand patches are attributed different the values $\beta_m=1.9$ and $\beta_c=1.1$, respectively. (a) Setup S2, (b) Setup S2I, (c) Setup S3, (d) Setup S4.

be matched by the scaling described in the Appendix.

The effect of varying t_2 on the breakthrough curves is shown in Fig. 5(b) for $\beta=1.7$ and $\beta=1.1$ in Fig. 5(d). The parameter t_2 controls the time when transport behavior evolves to Fickian. If t_2 is smaller than the time point of breakthrough, the breakthrough curve is entirely Fickian and matches exactly the ADE solution. The influence of t_2 weakens as β increases, because the transition to Fickian occurs earlier. For low β [Fig. 5(d)] and high t_2 one observes the largest range of power-law tail (non-Fickian behavior).

The response of the breakthrough curves to a variation of the inlet flow rate is shown in Fig. 6(a) for $\beta=1.1$ and Fig. 6(b) for $\beta=1.9$. For different inlet flow rates the ADE solutions can be matched by scaling the time according to the inlet flow ratio. The CTRW solutions are distinctly different for each flow rate (i.e., they cannot be simply scaled). We note three main features. First, the transition to the long tail occurs at lower concentrations for higher inlet flow rates (for larger β). Qualitatively the same behavior exists (not shown) for the uniform flow field. Second, for $t > t_2$ the breakthrough curves tend to Fickian behavior again, because the transit time distribution for $t > t_2$ is increasingly dominated by the exponential term. Third, because the β value for all inlet flow rates is the same, the slope of the tail for $t < t_2$ (the power-law region) is the same.

B. Composite medium

We now consider the composite media setups S3 and S4 and their “inverses” S3I and S4I as shown in Fig. 3. First, we compare transport in a composite medium to transport in a

uniform medium, upon variation of the inlet flow rate, by considering setups S2 to S4. Second, we demonstrate the effects of attributing different β values to different types of porous medium (medium sand, coarse sand). As seen from Fig. 3, interchanging the type of sand in setups S3 and S3I changes the hydraulic conductivity distribution and hence the flow lines (independent of the β values). We choose two widely differing β values, $\beta=1.1, 1.9$ and observe the breakthrough curves for all four possible combinations (β value, type of porous medium). In general, we assign higher β values to the medium sand, which has grain sizes smaller than the coarse sand. We argue that there probably exist more stagnant zones in a coarse sand than in a medium sand in a microscopic flow field; these zones lead to a transit time distribution for a migrating particle that is described by a longer tail and therefore by a lower value of β .

The comparison between uniform and composite media can be seen in Fig. 6. Figures 6(a) and 6(b) show the breakthrough curves for setups S2 and S2I, containing homogeneous uniform media of coarse sand and medium sand, respectively. Figures 6(c) and 6(d) show the breakthrough curves when a patch of medium sand is introduced in the center of the domain or adjacent to the outlet. Comparing Figs. 6(a) and 6(c), a clear difference between uniform (S2) and composite (S3) media is apparent in the tailing of the breakthrough curves. The slope in the tail for the homogeneous media remains the same until it reaches the exponential cutoff time t_2 ; for the composite medium, we observe a slower increase in concentration and therefore a decrease in the absolute value of the slope. It is interesting to note that upon variation in the inlet flow rate in the composite medium

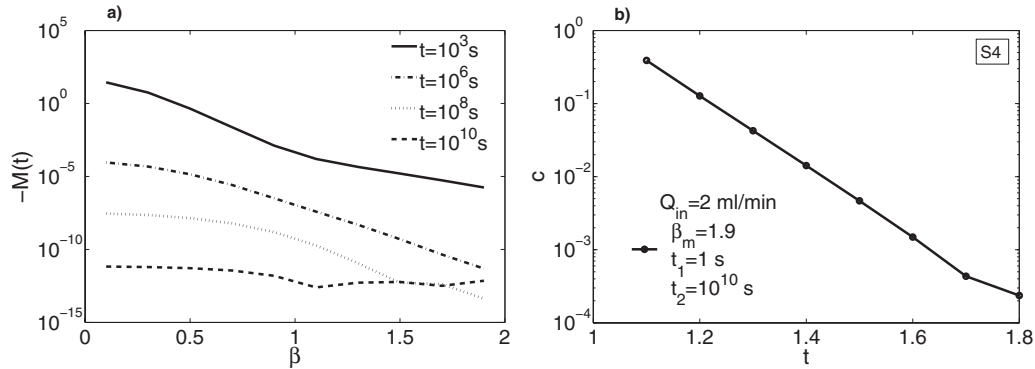


FIG. 7. Maximum concentration (mol/cm²) at the outlet in setup S4 as a function of value of β_c and the memory function $M(t)$ (1/s) as a function of value of β . Parameters t_1 and t_2 are chosen as in Fig. 6. (a) Memory function for different time points; (b) $Q_{in}=2$ ml/min.

(setup S3), all breakthrough curves converge at long times [Fig. 6(c)]. For the time range shown, such behavior is not apparent for breakthrough curves from uniform media filling [Figs. 6(a) and 6(b)].

In the composite domains, the transport equation indicates that mass accumulates in the domain, in the vicinity of the inner patch. This phenomenon can be seen clearly in the breakthrough curves [Fig. 6(d)] for the domain in which the patch is shifted adjacent to the outlet (setup 4). Recall that in setup S4, the patch (light color) consists of medium sand ($\beta_m=1.9$) while the surrounding region is coarse sand (dark color) with $\beta_c=1.1$. This mass accumulation is due purely to the existence of an “interface” in the β value; more precisely it is due to a nonvanishing spatial first-order derivative of the memory function, and its sign, in the transport Eq. (25). For setup S4 and with the β values as assigned in Fig. 6, the sign of $\partial M(x,t)/\partial x$ is positive at the interface at $x=13.8$ cm. The y derivative of $M(x,t)$ is positive at $y=6.9$ cm and negative at $y=18.1$ cm. Figure 7(a) shows $M(t)$ as a function β for different time points; note that essentially $\partial M(t)/\partial \beta \geq 0$.

Figure 6(d) shows maximum concentrations as large as 1.66 times the inlet concentration. To examine further, we determined [Fig. 7(b)] the maximum concentration of the breakthrough curve (for setup S4) as a function of the value of β_c . It is clear that as the ratio between values of β_c and β_m decreases, the maximum concentration decreases sharply. For $\beta_c=1.8$ and $\beta_m=1.9$, which are realistic values in many experiments [e.g., [9]], the maximum concentration is only 1.0002; such measurement resolution is not readily achieved in laboratory experiments on transport in porous media. Mass accumulation in the domain is also clearly visible from inspection of plots showing concentration profiles in setup S3 (Fig. 8). Note that in all three cases shown in Fig. 8, the long time concentration converges to unity, the value of the inlet concentration (recall Sec. III B). In accord with the behavior shown in Fig. 7(b), the relative amount of mass accumulation decreases as the value of β_c approaches that of β_m . Observe also that the mass accumulates in the region with the higher value of β .

We now consider a detailed comparison of breakthrough curves for the composite media (setups S3, S3I, S4, S4I), for all possible combinations of β values and porous medium types, with the constraint $\beta_c \neq \beta_m$. These combinations are considered independent of our previous assignment of higher

β values to the sand type with smaller grain size. Figure 9 shows the effects of these combinations upon breakthrough curves in the four composite media. The plots show the breakthrough curves (outlet concentrations) and the average resident concentration within the inner patch of porous medium. From Figs. 9(b) and 9(d), it is seen that when the inner patch is attributed the higher β value, regardless of the type of porous media (coarse or medium sand), and thus regardless of the specific velocity flow field (recall the streamlines shown in Fig. 3), mass accumulates within the inner patch (as noted above, considering Fig. 8). On the other hand, mass is depleted in the inner patch, relative to the ADE solution, when the inner patch is assigned the lower β value.

We note also that the inlet and outlet boundary conditions for setups S3 and S3I are such that connected flow paths exist within a single type of porous media; particles need not cross an interface. In contrast, all flow paths in setups S4 and S4I must cross an interface. All breakthrough curves in setups S4 and S4I demonstrate the accumulation effect when the inner patch is assigned the higher β value; as a consequence, breakthrough curves [Fig. 9(c)] and average resident concentrations (Fig. 9(d)) are similar.

The CTRW picture of the particle transport was applied originally to hopping: a sequence of discrete transitions in time and space. We have adapted this picture for the particles moving in a fluid. The flow field is a totally passive background supplying a complex network of channels with velocity $\mathbf{v}(\mathbf{x})$. For the pore network, the channels are interporous throats. In sequence, each particle moves by traversing these channels. The slower channels act similarly to the effects of traps or physisorption against the faster ones that act like “mobile” particles. The difference in these mechanisms is the spectrum of the channels. The concentration in this picture can vary in a uniform (statistically homogeneous) medium like dissolved particles in fluid volumes, wherein the initial inlet concentration is the upper bound on concentration within the domain. However in a composite medium, different features can be introduced, such as a “macrorepository.” In this case, the particles seem to be “attracted” into the inner patch by the gradient of $M(t; \mathbf{x})$. It is important to recall that $M(t; \mathbf{x})$ acts like a nonlocal in time “velocity,” in that it acts mathematically to affect both \mathbf{v} and \mathbf{D} . The nonlocality provides accumulation: the inner patch itself acts as a temporary repository, and the larger β acts on the sign of $M(t; \mathbf{x})$. The

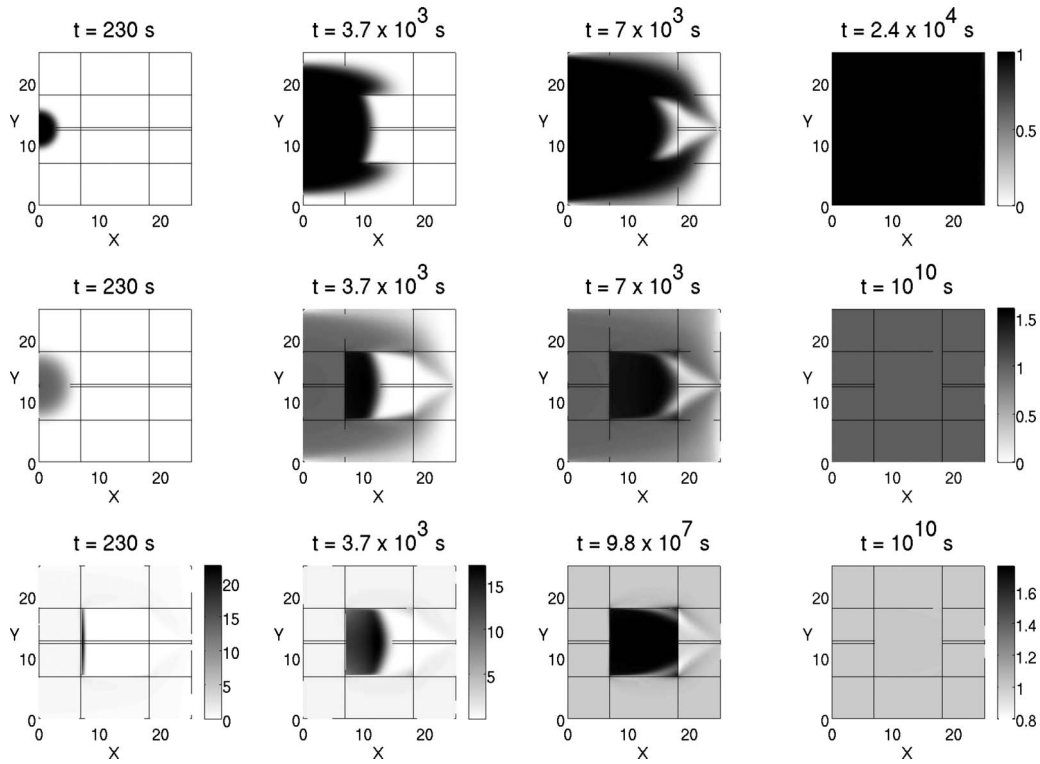


FIG. 8. Spatial concentration distribution $[x, y \text{ (cm)}]$ at different times for setup S3 (recall Fig. 3). First row: ADE solution. Second row: CTRW solution for $t_c = \bar{t}$ with parameters $t_1 = 1 \text{ s}$, $t_2 = 10^{10} \text{ s}$, $\beta_c = 1.1$, and $\beta_m = 1.9$. Third row: CTRW solution for $t_c = \bar{t}$ with parameters $t_1 = 1 \text{ s}$, $t_2 = 10^{10} \text{ s}$, $\beta_c = 0.8$ and $\beta_m = 1.9$. Note the different concentration scale bars in each row.

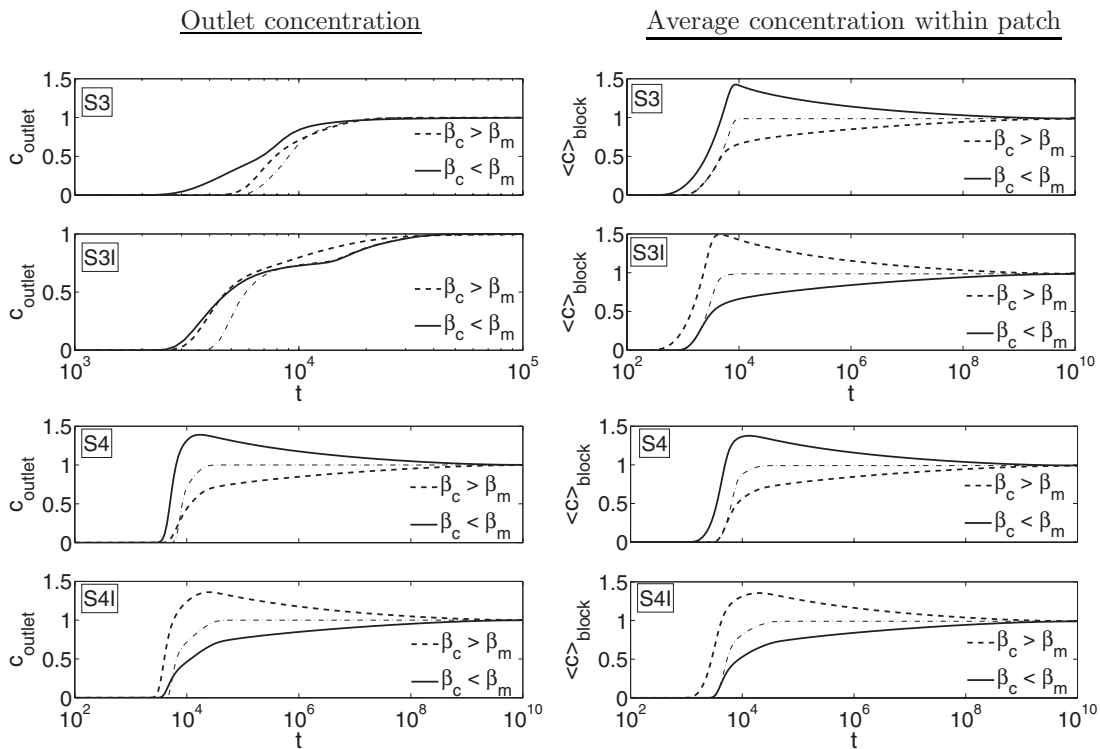


FIG. 9. All combinations of porous media type (subscripts c and m denote coarse and medium sand, respectively) with $\beta = 1.1, 1.9$ (recall Fig. 3). For comparison, the thinner dotted-dashed line represents the ADE solution. Shown are concentrations (mol/cm²) over time (s) at the outlet (left column) and averaged over the inner patch (right column) for setups S3, S3I, S4, and S4I.

significance of the abrupt shift in β values at the internal interface can be viewed in the context of the effect it has on the nature of tracer pulse propagation. The value of β dominates the shape of this pulse; for lower β the pulse is more spread out (non-Gaussian) and for β approaching $\beta=2$ the pulse approaches a more concentrated (Gaussian) form. This localized change in the pulse shape can induce a readjustment that results in this case in a transient mass accumulation.

We have found the CTRW picture excellent for statistically homogeneous media, but its application to composite media remains a subject of investigation. Exploring the richness of the solutions of Eq. (25) in a parameter space (including the attribution of higher β values to finer sand in a large-scale composite medium) and in different composite configurations provide predictions for laboratory experiments, especially for possible accumulation effects. However, as noted above, firm experimental evidence for this effect is not currently available, and design of appropriate high-resolution, high β -contrast experiments remain to be carried out.

V. SENSITIVITY ANALYSIS

The CTRW equation has been derived from the ensemble average of Eqs. (2) and (5), which is equivalent to the master equation (1). The variance of the ensemble average of $c(\mathbf{s}, t)$, Eq. (3), is an important consideration in assessing the uncertainties involved in replacing the $c(\mathbf{s}, t)$ for a specific realization (a given field site) by $\langle c(\mathbf{s}, t) \rangle$. As discussed in Sec. 5 of [9], the variance is determined largely by the relation between the system size L and the scale λ of the heterogeneities. For the case $L < \lambda$, we have developed the hybrid method Sec. 4 of [9], in which the ensemble average is limited to the smaller scale part of the distribution of heterogeneities. Even in the context of $L > \lambda$, there remains the uncertainty of replacing the average of $\psi_{\mathbf{s}-\mathbf{s}', s'(t-t')}\mathcal{R}(\mathbf{s}', t')$ by $\psi(\mathbf{s}-\mathbf{s}', t-t') \langle \mathcal{R}(\mathbf{s}', t') \rangle$.

We examine this uncertainty by the physically motivated feature of a correction to the ensemble average of Eq. (5), $\delta\psi(\mathbf{s}, t)$, which induces a correction $\delta R(\mathbf{s}, t)$ to $\langle \mathcal{R}(\mathbf{s}, t) \rangle$ [designated in the following as $R_c(\mathbf{s}, t)$],

$$R_c(\mathbf{s}, t) + \delta R(\mathbf{s}, t) = \sum_{\mathbf{s}'} \int_0^t [\psi(\mathbf{s}-\mathbf{s}', t-t') + \delta\psi(\mathbf{s}-\mathbf{s}', t-t')] \times [R_c(\mathbf{s}', t') + \delta R(\mathbf{s}', t')] dt'. \quad (30)$$

To lowest order, we have the CTRW equation

$$R_c(\mathbf{s}, t) = \sum_{\mathbf{s}'} \int_0^t \psi(\mathbf{s}-\mathbf{s}', t-t') R_c(\mathbf{s}', t') dt' \quad (31)$$

and the coupled one

$$\delta R(\mathbf{s}, t) = \sum_{\mathbf{s}'} \int_0^t \{ \delta\psi(\mathbf{s}-\mathbf{s}', t-t') R_c(\mathbf{s}', t') + [\psi(\mathbf{s}-\mathbf{s}', t-t') + \delta\psi(\mathbf{s}-\mathbf{s}', t-t')] \delta R(\mathbf{s}', t') \} dt'. \quad (32)$$

We can solve Eq. (32) using the Laplace and Fourier transforms,

$$\delta \tilde{R}(\mathbf{k}, u) = \frac{\delta \Lambda(\mathbf{k}, u) \tilde{R}_c(\mathbf{k}, u)}{1 - \Lambda(\mathbf{k}, u) - \delta \Lambda(\mathbf{k}, u)} \quad (33)$$

with

$$\tilde{R}_c(\mathbf{k}, u) = \frac{1}{1 - \Lambda(\mathbf{k}, u)} \quad (34)$$

and with $\tilde{R}_c(\mathbf{k}, u)$, $\Lambda(\mathbf{k}, u)$, $\delta \tilde{R}(\mathbf{k}, u)$, and $\delta \Lambda(\mathbf{k}, u)$ the Laplace and Fourier transforms of $R_c(\mathbf{s}, t)$, $\psi(\mathbf{s}, t)$, $\delta R(\mathbf{s}, t)$, and $\delta\psi(\mathbf{s}, t)$, respectively. The relation in Eq. (33) can be simplified by dropping $\delta \Lambda(\mathbf{k}, u)$ in the denominator to read

$$\delta \tilde{R}(\mathbf{k}, u) = \delta \Lambda(\mathbf{k}, u) \tilde{R}_c^2(\mathbf{k}, u). \quad (35)$$

Hence, multiplying by $[1 - \psi(u)]/u$ we obtain

$$\delta \tilde{c}(\mathbf{k}, u) = \delta \Lambda(\mathbf{k}, u) \tilde{R}_c(\mathbf{k}, u) \tilde{c}(\mathbf{k}, u), \quad (36)$$

so that,

$$\delta c(\mathbf{s}, t) = \sum_{\mathbf{s}'} \int_0^t \delta F(\mathbf{s}-\mathbf{s}', t-t') c(\mathbf{s}', t') dt'. \quad (37)$$

where

$$\delta F(\mathbf{s}, t) = \sum_{\mathbf{s}'} \int_0^t \delta\psi(\mathbf{s}-\mathbf{s}', t-t') R_c(\mathbf{s}', t') dt'. \quad (38)$$

The relations in Eqs. (37) and (38) determine the sensitivity of the concentration $c(\mathbf{s}, t)$ to an uncertainty or correction to $\psi(\mathbf{s}, t)$. The uncertainty in $\psi(\mathbf{s}, t)$ can arise from a number of sources, a prime one being the uncertainty in the velocity histogram $\Phi(\xi)$, $\xi \equiv 1/v$. In a porous medium one determines $\Phi(\xi)$ based on an assumed length scale ℓ , which for practical reasons is larger than the pore scale. One can use the $\delta\psi(\mathbf{s}, t)$ generated by variations of ℓ for specific permeability fields as a basis for calculating $\delta c(\mathbf{s}, t)$.

VI. CONCLUSIONS

The basic idea of using a CTRW framework to describe transport in a disordered system relies on a mapping of all the fluctuations of the local transition times and displacements in an ensemble of the realizations of the system onto a joint distribution $\psi(\mathbf{s}, t)$. This is accomplished by the ensemble average of Eq. (1), or more specifically, of Eq. (5). The resultant CTRW equations are homogeneous in space. The FADE is a subset of the CTRW framework—the order of the derivative operators depends on a pure power-law form of $\psi(t)$. Unlike the universal character of the standard partial differential equations of physics, the form of the fractional derivative equations analyzed herein is related to the properties of the system under investigation, e.g., β . Any significant change in the ensemble average of the system, such as the addition of an external potential changes the physical basis of the CTRW and FADE transport equations. The form of the fractional Fokker-Planck equation exhibits a

decoupling between the external potential $V(\mathbf{x})$ and the transition rates of the disordered system that the fractional derivatives represent.

In Sec. III we approach, in principle, the problem of a system containing heterogeneities on all scales. For the part of the latter distribution whose size is greater than λ we can solve for the steady-state flow field $\mathbf{v}(\mathbf{x})$. For the rest of the size class of heterogeneities less than λ we treat these regions probabilistically. Essentially we represent these local regions as an ensemble average which determines a $\psi(\mathbf{s}, t; \mathbf{x})$ as in Sec. II. However, the $\psi(\mathbf{s}, t)$ is now position dependent. The length λ is determined pragmatically in analyzing an hydraulic conductivity field; it represents the limits of resolution of the disorder.

We derive the transport Eq. (25) with this construct, suggesting that this equation can be used to handle the problem raised in Sec. II of dealing with an irreducible nonstationarity due to a force field or a macroscopic flow field. The disorder and the latter are coupled. We have now introduced position-dependent parameters related to the disorder, e.g., $\beta(\mathbf{x})$. Equation (25) is solved for various arrangements of porous media with different boundary conditions and a range of memory function (21) parameters. Variation of the latter produces significant changes in the dynamics of the concentration profiles. A crucial feature affecting the nature of the solutions of Eq. (25) is the direction of the spatial gradient of the memory function at interfaces of the composite medium. Depending on this spatial behavior of $\tilde{M}(u; \mathbf{x})$, e.g., $\beta(\mathbf{x})$, one obtains regions of mass accumulation or depletion. This is clearly one enrichment in the possible solutions of Eq. (25); others remain to be explored.

Hence, local disorder has a strong effect on macrobehavior. The subtlety of choosing the physically meaningful value for $t_c(\mathbf{x})$ to produce the correct asymptotic concentration profile is discussed in detail. A treatment of the ADE is included in our full 2D analysis and its solutions are shown to fit breakthrough curves with long tails in uniform media. Further studies will include experiments testing the predictions

of the behavior of $c(\mathbf{x}, t)$ in composite media and in highly heterogeneous systems with the corresponding solutions of Eq. (25).

ACKNOWLEDGMENTS

The financial support of the European Commission (Contract No. PITN-GA-2008-212298) is gratefully acknowledged. The authors thank Guy Katz for carrying out the laboratory experiment.

APPENDIX: SCALING

In a uniform medium all parameters of the memory function, as well as porosity and dispersivity, are constant over the entire space. The memory function $M(t, t_1, t_2, \beta)$ in Laplace space can be written as

$$\tilde{M}(u, t_1, t_2, \beta) = \frac{t_c}{t_1} \frac{u t_1 f(u t_1 - \tau_2^{-1})}{f(\tau_2^{-1}) - f(u t_1 - \tau_2^{-1})}$$

with $\tau_2 = t_2/t_1$ and $f(u) = u^\beta e^{u\Gamma(-\beta, u)}$. The following relation for the memory function is true, which can be verified easily by taking the Laplace transform on both sides:

$$M(t, t_1, t_2, \beta) = M\left(\frac{t}{t_1}, 1, \frac{t_2}{t_1}, \beta\right)/t_1,$$

$$\tilde{M}(u, t_1, t_2, \beta) = \tilde{M}\left(u t_1, 1, \frac{t_2}{t_1}, \beta\right).$$

Therefore the transport equation transforms when changing to the dimensionless time $\tau = t/t_1$ according to

$$\frac{n}{t_1} \frac{\partial C(\mathbf{x}, \tau t_1)}{\partial \tau} = -\nabla \int_0^\tau M(\tau - \tau', 1, \tau_2, \beta) [\mathbf{q}(\mathbf{x}) C(\mathbf{x}, \tau' t_1) - |\mathbf{q}(\mathbf{x})| \alpha \nabla C(\mathbf{x}, \tau' t_1)] d\tau',$$

which leads to a dimensionless transport equation with $\tau = t/t_1$, $\tau_2 = t_2/t_1$, and $\mathbf{q}_\tau = \mathbf{q} t_1$.

-
- [1] E. W. Montroll and G. H. Weiss, *J. Math. Phys.* **6**, 167 (1965).
 [2] H. Scher and M. Lax, *Phys. Rev. B* **7**, 4491 (1973).
 [3] H. Scher and M. Lax, *Phys. Rev. B* **7**, 4502 (1973).
 [4] E. W. Montroll and H. Scher, *J. Stat. Phys.* **9**, 101 (1973).
 [5] H. Scher and E. W. Montroll, *Phys. Rev. B* **12**, 2455 (1975).
 [6] Y. Hatano and N. Hatano, *Water Resour. Res.* **34**, 1027 (1998).
 [7] G. Drazer, M. Rosen, and D. H. Zanette, *Physica A* **283**, 181 (2000).
 [8] G. Kosakowski, *J. Contam. Hydrol.* **72**, 23 (2004).
 [9] B. Berkowitz, A. Cortis, M. Dentz, and H. Scher, *Rev. Geo-phys.* **44**, RG2003 (2006).
 [10] Y. W. Xiong, G. H. Huang, and Q. Z. Huang, *J. Contam. Hydrol.* **86**, 163 (2006).
 [11] J. C. Deng, X. Jiang, X. X. Zhang, W. Hu, and J. W. Crawford, *Chemosphere* **71**, 2150 (2008).
 [12] M. E. Rhodes, B. Bijeljic, and M. J. Blunt, *Adv. Water Resour.* **31**, 1527 (2008).
 [13] R. Metzler, E. Barkai, and J. Klafter, *Physica A* **266**, 343 (1999).
 [14] E. Barkai, *Phys. Rev. E* **63**, 046118 (2001).
 [15] L. Friedman and T. D. Holstein, *Ann. Phys. (N.Y.)* **21**, 494 (1963).
 [16] J. Klafter and R. Silbey, *Phys. Rev. Lett.* **44**, 55 (1980).
 [17] A. Cortis, Y. Chen, H. Scher, and B. Berkowitz, *Phys. Rev. E* **70**, 041108 (2004).
 [18] M. Abramowitz and I. Stegun, *Handbook of Mathematical Functions* (Dover Publications, Inc., New York, 1970).
 [19] M. Dentz, H. Scher, D. Holder, and B. Berkowitz, *Phys. Rev. E* **78**, 041110 (2008).
 [20] R. Metzler and J. Klafter, *J. Phys. A* **37**, R161 (2004).
 [21] B. Berkowitz, J. Klafter, R. Metzler, and H. Scher, *Water Resour. Res.* **38**, 1191 (2002).

- [22] H. Risken, *The Fokker-Planck Equation: Methods of Solution and Applications*, Springer Series in Synergetics Vol. 18, 2nd ed. (Springer, Berlin, 1989).
- [23] R. Metzler and J. Klafter, Phys. Rep. **339**, 1 (2000).
- [24] S. Rackovsky and H. Scher, Phys. Rev. Lett. **52**, 453 (1984).
- [25] H. Scher and S. Rackovsky, J. Chem. Phys. **81**, 1994 (1984).
- [26] A. Cortis, C. Gallo, H. Scher, and B. Berkowitz, Water Resour. Res. **40**, W04209 (2004).
- [27] H. Scher, J. Phys. (Paris), Colloq. **42**, C4-547 (1981).
- [28] E. Barkai and V. N. Fleurov, Phys. Rev. E **58**, 1296 (1998).
- [29] M. Levy and B. Berkowitz, J. Contam. Hydrol. **64**, 203 (2003).
- [30] B. Berkowitz and H. Scher, Adv. Water Resour. **32**, 750 (2009).
- [31] A. V. Chechkin, R. Gorenflo, and I. M. Sokolov, J. Phys. A **38**, L679 (2005).
- [32] N. van Kampen, *Stochastic Processes in Physics and Chemistry* (Elsevier, New York, 2007).
- [33] B. Berkowitz, S. Emmanuel, and H. Scher, Water Resour. Res. **44**, W03402 (2008).
- [34] M. Dentz, A. Cortis, H. Scher, and B. Berkowitz, Adv. Water Resour. **27**, 155 (2004).
- [35] W. Kinzelbach, *Groundwater Modeling: An Introduction with Sample Programs in BASIC* (Elsevier, New York, 1986).
- [36] F. R. de Hoog, J. H. Knight, and A. N. Stokes, SIAM J. Sci. Comput. (USA) **3**, 357 (1982).
- [37] B. Berkowitz and Group, CTRW MATLAB TOOLBOX (ESER, June 2008), URL <http://www.weizmann.ac.il/ESER/People/Brian/CTRW/>
- [38] S. E. Silliman and E. S. Simpson, Water Resour. Res. **23**, 1667 (1987).
- [39] J. Luo, M. Dentz, O. Cirpka, and P. Kitanidis, Water Resour. Res. **43**, W09403 (2007).